ANTHROPOLOGY

Cranial endocast of a stem platyrrhine primate and ancestral brain conditions in anthropoids

Xijun Ni[1,2,3,4]*, John J. Flynn[2], André R. Wyss[5], Chi Zhang[1,3]

Understanding of ancestral conditions for anthropoids has been hampered by the paucity of well-preserved early fossils. Here, we provide an unprecedented view of the cerebral morphology of the 20-million-year-old *Chilecebus carrascoensis*, the best-preserved early diverging platyrrhine known, obtained via high-resolution CT scanning and 3D digital reconstruction. These analyses are crucial for reconstructing ancestral brain conditions in platyrrhines and anthropoids given the early diverging position of *Chilecebus*. Although small, the brain of *Chilecebus* is not lissencephalic and presents at least seven pairs of sulci on its endocast. Comparisons of *Chilecebus* and other basal anthropoids indicate that the major brain subdivisions of these early anthropoids exhibit no consistent scaling pattern relative to the overall brain size. Many gross cerebral features appear to have transformed in a mosaic fashion and probably have originated in platyrrhine and catarrhine anthropoids independently, involving multiple, independent instances of size increase, as well as some secondary decreases.

INTRODUCTION

It is only natural for *Homo sapiens*, the most inquisitive of anthropoids, to seek to unravel the evolution of intelligence and brain structure in its closest kin. The evolution of the brain in primates has long been investigated from anatomical, physiological, and behavioral perspectives (*1*–*4*), while recent molecular studies have begun to reveal the genomic underpinnings of its complex transformations. Mutations of regulatory genes (*microcephalin* and *ASPM*), for example, are implicated in primary microcephaly in humans, a phenotype widely considered atavistic, or reflective of an earlier evolutionary stage in hominid history (*5*, *6*). Although certain features of the ancestral primate brain may be deduced from the study of modern forms in a phylogenetic context, direct evidence pertinent to various evolutionary analyses and theories can only come from fossils (*1*, *2*).

The endocranial cast, or endocast, preserved within fossilized braincases, provides an invaluable window into the brain structure of ancient taxa. Fortuitously, mammalian endocasts provide not only general information about brain shape and size but also details about the position and form of cranial nerves, blood vessels, sinuses, and even sulcal patterns (*1*, *2*). Well-preserved endocasts often resemble the exterior of fresh brains covered in dura mater (*7*). Because natural endocasts of extinct primates are exceedingly rare, particularly for early anthropoids, knowledge of the "fossil brain" of key extinct forms is extremely limited. In exceptional preservational circumstances, however, endocasts of fossil anthropoids provide a rich repository of information essential for understanding brain evolution.

The two subgroups of crown anthropoids, platyrrhines (New World monkeys) and catarrhines (Old World monkeys and apes, including humans), have evolved many features in parallel since their divergence at least 36 million years (Ma) ago (*8*). Some platyrrhines, such as tool-using capuchins, have remarkably enlarged brains relative to their body mass (*9*). Although the brains of extant platyrrhines are well studied (*10*), ancestral conditions for the group remain poorly understood, in large part, because of the scarcity of skulls and endocasts of early fossil forms. Among the rare pre-Pleistocene platyrrhine skulls known, brain structure has been investigated only in *Dolichocebus gaimanensis* on the basis of cursory inspection of the eroded skull surface exposing the endocast (*1*).

Herein, we present results of the first high-resolution computed tomography (CT) scanning study of the endocranial morphology of *Chilecebus carrascoensis* and analyses of virtual three-dimensional (3D) reconstructions deriving therefrom. *C. carrascoensis*, from early Miocene (20.09 Ma) volcaniclastic deposits of the central Andes, known from a single skull (SGOPV 3213), is by many measures the best-preserved Neogene platyrrhine known (*11*). On the basis of the most comprehensive haplorhine primate data matrix assembled to date (comprising 60 taxa and 1844 characters, including 473 dental, 201 cranial, 309 postcranial, 203 soft tissue, and 658 short and long interspersed nuclear elements), we conducted phylogenetic analyses of the group via Bayesian inference and parsimony analysis. *Chilecebus* was identified as one of the earliest diverging stem platyrrhines known (figs. S1 to S3), thereby making this taxon especially important for assessing ancestral cerebral features for the clade.

RESULTS

Endocast of *Chilecebus*

On the basis of direct digital volumetric reconstructions from high-resolution x-ray CT scans, the endocast of *Chilecebus* (Fig. 1 and fig. S4) occupies 7862 mm^3, near previous indirect estimates (*11*, *12*). A modern brain of this volume would weigh 7.96 g.

In dorsal view, the endocast of *Chilecebus* is egg shaped (Fig. 1A and fig. S4A), and the frontal pole is narrower than the occipital. The frontal lobe does not overlap the olfactory bulbs. The wide occipital portion forms the endocast's rounded posterior end and completely covers the cerebellum.

The frontal lobe is a little expanded dorsally, making the anterodorsal part of the endocast fairly flat (Fig. 1, B and C, and fig. S4, B and C). The temporal portion is distinctly expanded ventrally, forming

[1]Key Laboratory of Vertebrate Evolution and Human Origins, Institute of Vertebrate Paleontology and Paleoanthropology, Chinese Academy of Sciences, 142 Xi Zhi Men Wai Street, Beijing 100044, China. [2]Division of Paleontology and Richard Gilder Graduate School, American Museum of Natural History, Central Park West at 79th Street, New York, NY 10024, USA. [3]CAS Center for Excellence in Life and Paleoenvironment, Beijing 100044, China. [4]University of Chinese Academy of Sciences, Beijing 100049, China. [5]Department of Earth Science, University of California, Santa Barbara, Santa Barbara, CA 93106, USA.
*Corresponding author. Email: nixijun@ivpp.ac.cn

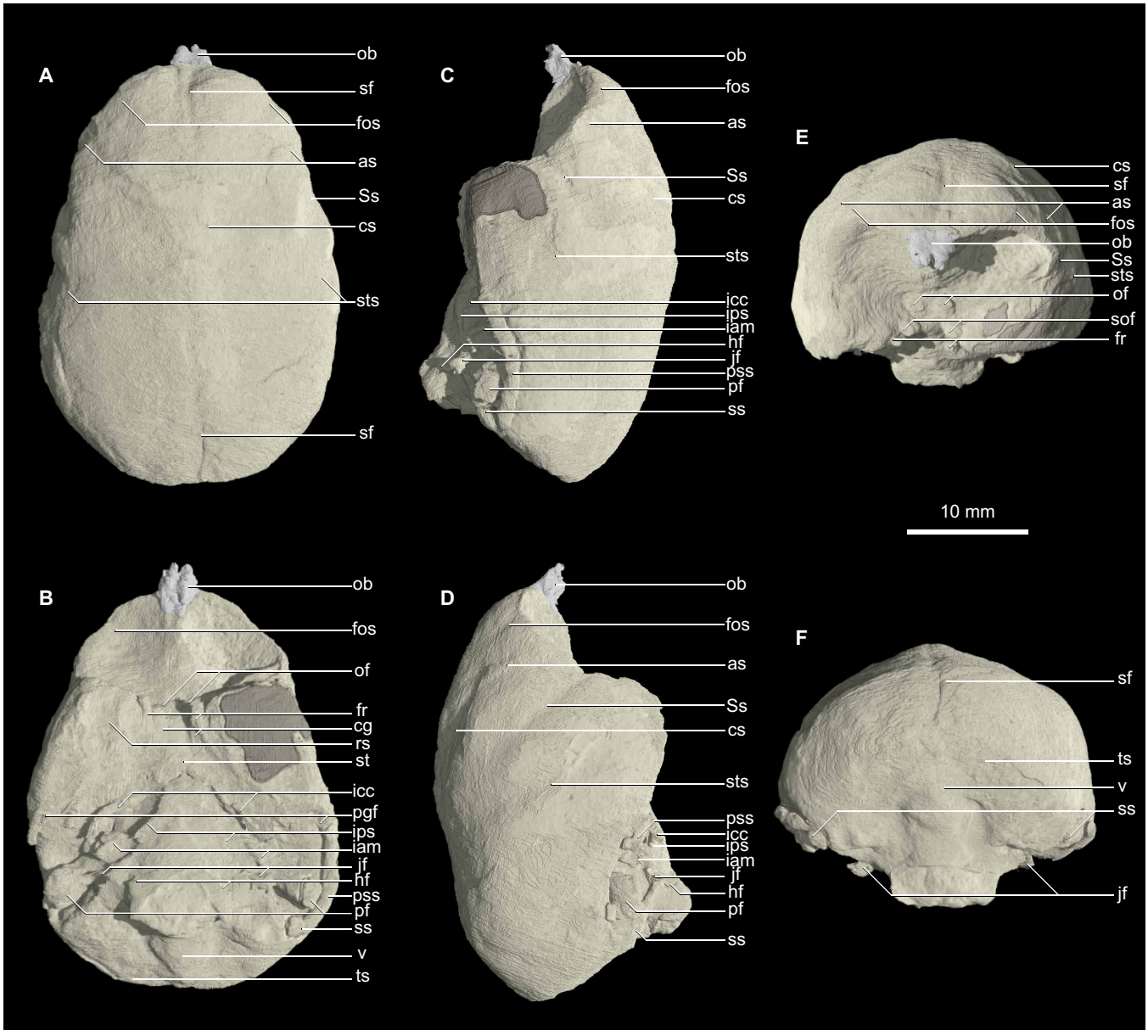

Fig. 1. Virtual cranial endocast of *Chilecebus* based on high-resolution CT scanning images. Gray shadows indicate reconstructed portions. (**A**) Dorsal. (**B**) Ventral. (**C**) Left lateral. (**D**) Right lateral. (**E**) Anterior. (**F**) Posterior. as, arcuate sulcus; cg, cavernous groove; cs, central sulcus; fos, fronto-orbital sulcus; fr, foramen rotundum; hf, hypoglossal foramen; iam, internal acoustic meatus; icc, internal carotid canal; ips, inferior petrosal sinus; jf, jugular foramen; ob, olfactory bulb; of, optic foramen; pf, parafloccullus; pgf, postglenoid foramen; pss, petrosquamous sinus; rs, rhinal sulcus; sf, sagittal fissure; sof, superior orbital fissure; Ss, Sylvian sulcus; ss, sigmoid sinus; st, sella turcica; sts, superior temporal sulcus; ts, transverse sulcus; v, vermis.

a rounded lobe. The dorsal profile of the parietal portion of the endocast is nearly horizontal and subtly saddle shaped, as the occipital and the posterior part of the frontal lobes are slightly elevated over the parietal area. Although the occipital lobe is expanded posteriorly and laterally relative to the cerebellum, its posterior surface is relatively flat. The paraflocculus of the cerebellum appears as a distinct thumb-like eminence ventral to the lateral border of the occipital lobe.

Ventrally, the olfactory peduncles are present as two short narrow ridges corresponding to a depression on the ethmoid roof, which, in life, housed the two olfactory tracts posteriorly (Fig. 1D and fig. S4D). Lateral to the olfactory peduncles and anterior to the temporal lobes, two large concavities beneath the frontal lobes accommodated the deep orbits. The ventral surface of the temporal lobe is generally flat. The temporal lobes occupy ~40% of the width of the ventral surface of the endocast at their widest point. The space between the two temporal lobes is narrow. At the center of this region, a low, oval, ventrally projecting bulge represents the sella turcica (hypophyseal fossa). Posterior to the sella turcica, a narrow but deep indentation marks the dorsum sella and posterior clinoid process. Shallow depressions lateral to the sella turcica define the medial boundary of

the cavernous sinus. The cavernous sinus, a topographically irregular region, is traversed by numerous veins, nerves, and the internal carotid artery. Posterior to the cavernous sinuses and sella turcica lies the cast of the shallow groove of the basilar part of the occipital bone. This fairly broad, flat surface supports the pons and medulla oblongata.

The occipital lobes of the cerebrum and the posterior part of the cerebellum are visible in posterior view (Fig. 1F and fig. S4F). The centrally located vermis occupies approximately one-third of the posterior surface of the cerebellum. The cerebellar hemispheres are set apart from the vermis by two shallow, dorsomedially curving grooves.

The sulcal pattern of the brain is well preserved in *Chilecebus* (fig. S4). The sagittal fissure, which divides the cerebrum into left and right hemispheres, leaves a deep and broad depression on the frontal and occipital parts of the endocast. A short sulcus extends posteromedially along the anterolateral border of each frontal lobe. The position of this structure suggests that it represents the dorsal extension of the fronto-orbital sulcus. A rectus sulcus typically occurs in this region in modern primates, where it parallels (rather than crosses) the orbital margin of the frontal lobe. In *Chilecebus*, these dorsal sulci traverse the orbital margin of the frontal lobe but ventrally are continuous with the fronto-orbital sulci (particularly clearly visible on the better-preserved right side). Posterior to these dorsal extensions of the fronto-orbital sulci, a pair of long, prominent sulci originates near the sagittal fissure, about one-third the length of the endocast from the anterior pole of the frontal lobe, and then course anterolaterally (best seen in Fig. 1C and fig. S4C). The position and shape of these paired structures suggest that they represent central sulci. They curve and diverge anterolaterally for a considerable distance, at which point they turn sharply laterally to join much straighter sulci. These latter furrows, interpreted as the arcuate sulci (equal to inferior precentral sulci), approach the lateral border of the frontal lobe. Prominent Sylvian sulci lie posterior and ventral to the central and arcuate sulci, course posterodorsally, and divide the frontal and temporal lobes. On the temporal lobe, the superior temporal sulcus runs posterodorsally, roughly paralleling the Sylvian sulcus, but the former extends farther dorsally. A shallow groove crosses (anteroposteriorly) the ventral surface of the temporal lobe. This groove is likely the rhinal sulcus (Fig. 1D and fig. S4D), which separates the medial piriform cortex from the lateral neocortex of the cerebrum. The parietal and occipital portions of the endocast are smooth, lacking clear evidence of sulci.

Casts of the cranial nerves, vessels, and sinuses are best seen in ventral view. The cavernous sinus is continuous anteriorly with the canal-like cavernous groove, which, in turn, leads to the superior orbital fissure (Fig. 1, D and F, and fig. S4, D and F). Lateral to the cavernous groove is a thinner canal, round in cross section, representing the foramen rotundum (preserved on the right side only). Superomedial to the casts of the superior orbital fissure and foramen rotundum lie two circular cross sections, identified as the optic foramina.

Long canals diverge from either side of the posterior end of the cavernous sinuses; they extend posterolaterally from the lateral side of the posterior clinoid processes to the ventrolateral side of the internal acoustic meatus. These structures are interpreted as passages for the internal carotid artery (Fig. 1D and fig. S4D). Posterior to the cavernous sinuses and immediately lateral to the pons and medulla oblongata, the inferior petrosal sinuses are present as prominent longitudinal keels. These sinuses connect the cavernous sinuses anteriorly and the jugular foramen posteriorly. The jugular foramen indicates that this aperture was fairly large and opened anteriorly. The sigmoid sinuses also are visible in ventral view (Fig. 1D and fig. S4D). The conical internal acoustic meatus lies anteromedial to the paraflocculus. The hypoglossal foramen appears as a small projection medial to the jugular foramen and anterior to the foramen magnum.

A long, gently arched, tube-like structure spans the posterior end of the temporal lobe to the occipital region of the endocast, paralleling the lateral border of the cerebrum and passing directly above the paraflocculus. This feature is most completely preserved on the specimen's left side (Fig. 1B and fig. S4B). The position and form of this tube suggest that it is the petrosquamous sinus, a large intracranial venous drainage channel (*13*, *14*) that drains the sigmoid sinus via the postglenoid foramen. The petrosquamous sinus is typically present in extant strepsirrhines and tarsiers (*14*). Direct (i.e., impressions on fossil endocasts) and indirect (i.e., presence of a postglenoid foramen) evidence demonstrates that this sinus is more widely distributed, also occurring among adapiforms, omomyids, basal anthropoids, and most platyrrhines (*1*, *13*, *14*). The early stem platyrrhines *Dolichocebus*, *Tremacebus*, and *Homunculus* (*14*) all have a petrosquamous sinus, a feature absent in catarrhines but present in some crown platyrrhines. The petrosquamous sinus in *Chilecebus* is noteworthy for its large size and for being enclosed within a canal, the latter of which does not occur in crown platyrrhines.

Comparison with stem anthropoid, basal catarrhine, and other platyrrhine primates

The early Oligocene *Parapithecus grangeri* is generally regarded as a proximal outgroup of the minimally inclusive crown anthropoid clade including catarrhines and platyrrhines (*15*, *16*). The absolute endocast volume of *Parapithecus*, ~11,400 mm^3 (*16*), far exceeds that of *Chilecebus*. A virtual endocast based on high-resolution CT scanning images of a nearly complete skull of *Parapithecus* has been reported (*16*) but has not yet been described in detail. From published figures (*16*), we deduce that the endocast was virtually smooth and likely lissencephalic. The frontal lobe of *Parapithecus* appears lower and narrower than in *Chilecebus*. The frontal lobe of *Parapithecus* is barely expanded anteriorly over the large olfactory bulbs. In lateral profile, the occipital and parietal lobes of *Parapithecus* are not elevated relative to the cerebellum, suggesting that these portions of the brain are less expanded than in *Chilecebus*.

The endocranial cast of *Aegyptopithecus zeuxis*, a widely accepted stem catarrhine (*15*, *17*), is more than twice the absolute volume of the stem platyrrhine *Chilecebus* (*17*). Comparative lateral profiles of the endocasts of *Aegyptopithecus* and *Chilecebus* (fig. S5A) highlight their differences. The olfactory bulbs of *Aegyptopithecus* are much larger in proportion to the endocast as a whole. The occipital portion of the *Aegyptopithecus* endocast is less expanded than in *Chilecebus*, its dorsal margin not rising over that of the cerebellum. The temporal lobes of both taxa are similar in the degree of ventral expansion and size. The occipital lobe of *Chilecebus*, however, is more dorsally expanded than that of *Aegyptopithecus*, while the reverse is true of the frontal lobes. In *Aegyptopithecus*, the portion of the brain dorsal to the nasion-opisthocranion axis is larger than the portion ventral to it, whereas in *Chilecebus*, the reverse is true. Well-defined central, Sylvian, superior temporal, intraparietal, and lunate sulci are present in *Aegyptopithecus* (*1*, *18*). Its central sulcus is similar to, but more anteriorly positioned than, that of *Chilecebus*. The arcuate sulcus, apparently absent in *Aegyptopithecus*, is present in *Chilecebus*. The Sylvian sulcus of both taxa extends a similar distance dorsally, but the superior

temporal sulcus of *Aegyptopithecus* is much longer posterodorsally. The intraparietal and lunate sulci, present in many extant primates, are prominent in *Aegyptopithecus* but are absent in *Chilecebus*.

Although other pre-Pleistocene platyrrhine skulls are known, only very limited information from the endocast of a single taxon, *D. gaimanensis*, is available for comparison. Judging from the outline of the reconstructed endocast (*1*), the lateral profile of *Dolichocebus* closely matches that of *Chilecebus* (fig. S5B). The sulcal pattern of *Dolichocebus* is incompletely reconstructed, with only the Sylvian sulcus recognized (*1*). It originates in a position similar to that in *Chilecebus* but is more dorsoposteriorly expanded in *Dolichocebus*. It is uncertain whether the other sulci preserved in *Chilecebus* have counterparts in *Dolichocebus* because of inadequate sulcus preservation of the latter.

Among extant platyrrhines, the callitrichines are similar in absolute and relative brain size to *Chilecebus*. The general morphology of the endocast of *Chilecebus* is also very similar to the brains of extant callitrichines, particularly in lateral profile (fig. S5, C to E). The sulcal pattern in callitrichines appears to be among the least specialized of all anthropoids (*10*). Typically, only the Sylvian, superior temporal, and rectus sulci are present. In a few species, such as *Callithrix humeralifer* and *Saguinus fuscicollis*, the central, arcuate, and intraparietal sulci are also present. In dorsal view, the Sylvian and superior temporal sulci of callitrichines are usually longer (both absolutely and relatively) than those of *Chilecebus*.

Extant platyrrhines other than callitrichines all have much larger relative and absolute brain sizes than *Chilecebus*. In addition, the brain is much more dorsally expanded in modern platyrrhines than in *Chilecebus*, as highlighted by the comparison between the representative extant platyrrhine *Saimiri sciureus* (fig. S5F) and the low and flat-roofed braincase of *Chilecebus*. The frontal and occipital lobes of *Saimiri* are expanded substantially, as is the region between the frontal and occipital lobes. The temporal lobe of *Saimiri*, however, is proportionally smaller and narrower than in *Chilecebus*. As a result, in *Saimiri*, the portion of the brain below the nasion-opisthocranion axis is considerably smaller than the portion above the axis, opposite to the condition in *Chilecebus*. The sulcal patterns of extant atelids and cebine cebids are more complex than in *Chilecebus*.

Evolutionary change of the encephalization quotient

The encephalization quotient (EQ) is a widely used index of brain size scaled to body size (*19*). Traditionally, allometric brain-body size scaling is determined via linear regression. Sometimes, however, nonrandom associations of traits among species (e.g., between body mass and brain size) are influenced by common ancestry, particularly when the taxa are closely related. Accordingly, phylogenetic considerations must be accounted for in analyzing covariation between traits across taxa (*20*). Here, we use phylogenetic generalized least squares (PGLS) analysis to correct for phylogenetic nonindependence between data points (species) (*20*). Results show a significant allometric relationship between brain and body mass in anthropoids (Supplementary Materials). The allometric slope for catarrhines is slightly, but insignificantly, steeper than that for platyrrhines (Supplementary Materials).

The EQ derived from PGLS equations is here termed the phylogenetic EQ (PEQ). Crown platyrrhines and nonhominin crown catarrhines exhibit similar PEQ distributions (varying from 0.86 to 3.38 and from 1.60 to 3.89, respectively; Fig. 2). The PEQs of *Dryopithecus*, *Pan*, *Australopithecus*, *Paranthropus*, and *Homo* are much higher (4.65 to 13.46) than in other anthropoids; these five hominids are shown as outliers in the box-and-whisker plot (Fig. 2). The PEQ of *Chilecebus* (0.79) far exceeds those of the stem catarrhine *Catopithecus browni* (0.31) and stem anthropoid *Proteopithecus sylviae* (0.30) but is similar to that of another stem anthropoid *P. grangeri* (0.70) and the stem catarrhine *A. zeuxis* (0.65). It is also close to the range (0.70 to 0.76) of extant tarsiers, the nearest extant outgroup to anthropoids, but lower than that of all crown platyrrhines and catarrhines (Figs. 2 and 3).

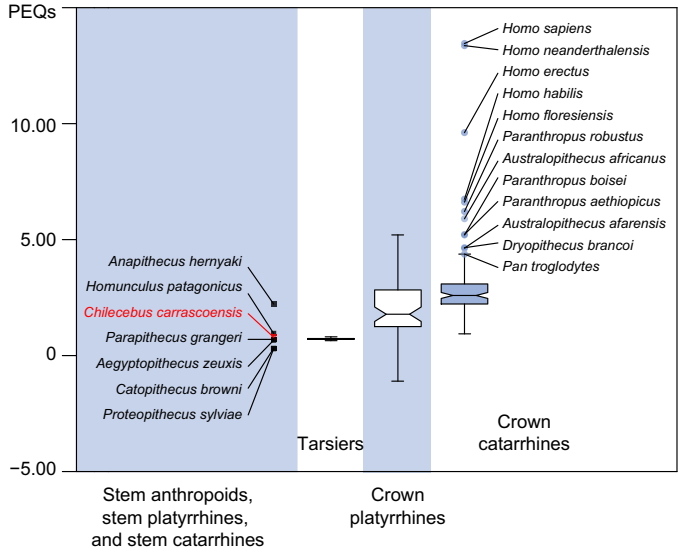

Fig. 2. Notched box-whisker plot of the PEQs of fossil and extant haplorhines. Whiskers show the lowest datum within 1.5 interquartile range (IQR) of the lower quartile and the highest datum within 1.5 IQR of the upper quartile. Outliers are shown as circles. For stem anthropoids, stem platyrrhines, and stem catarrhines, individual data points rather than the box and whisker are shown. PGLS regression for all anthropoids [x, ln(body mass); y, ln(brain weight); $y = 0.50x - 0.87$, $t = 12.22$, and $P < 0.001$) was used for calculating the PEQs. The PEQs of *Dryopithecus*, *Australopithecus*, *Paranthropus*, and *Homo* are much higher than in other anthropoids, shown as outliers.

The remarkably low PEQs of stem anthropoids are highlighted by mapping these values onto a phylogeny using maximum likelihood estimations and Bayesian inference of the ancestral states at the internal nodes; they even lag the PEQ of the extant tarsiers, the sister group of anthropoids (Fig. 3 and fig. S6). The similarly low PEQs of *Chilecebus* and *Aegyptopithecus* almost certainly typify both platyrrhines and catarrhines ancestrally and thus also anthropoids. Crown clade platyrrhines and catarrhines are both typified by substantially higher PEQs, making it difficult to escape the conclusion that these two groups of anthropoids convergently achieved increased levels of encephalization. Some platyrrhines (various cebines, pitheciines, and atelines), some hylobatids, and cercopithecine catarrhines also became even more highly encephalized (PEQs ~3 to 4) independently. Hominids stand out among anthropoids for their extremely high PEQs, the lineage including humans, the Hominini, being particularly notable in this regard (PEQs >4; Fig. 3 and fig. S6).

Although a general trend of increasing PEQ pervades the anthropoid phylogenetic tree, some clades exhibit pronounced PEQ decreases. This "counter-trend" is particularly clear among platyrrhines, with callithrichines, *Alouatta*, *Callicebus*, and some species of *Aotus*, showing significant PEQ drops compared to their sister taxa and inferred ancestral conditions.

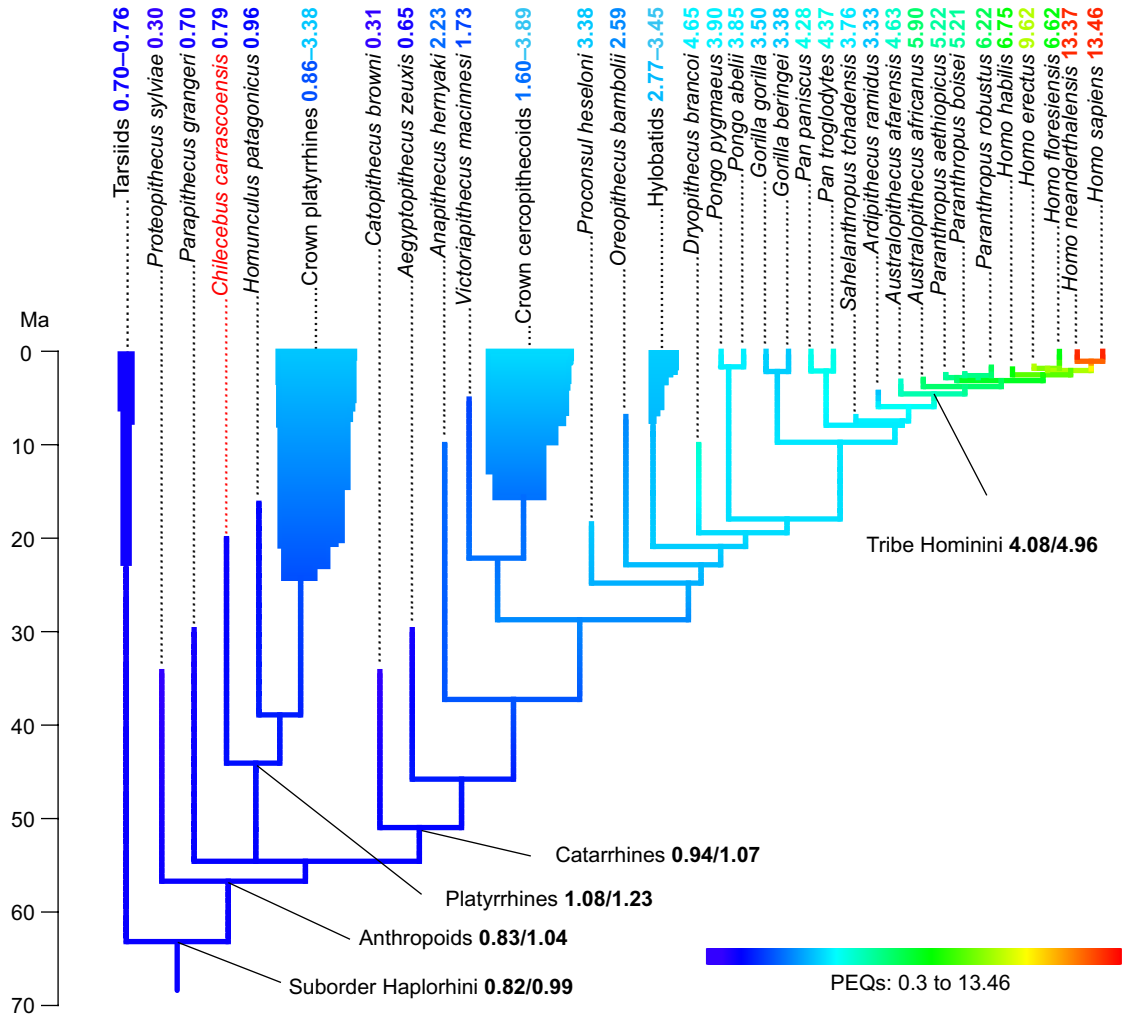

Fig. 3. Evolutionary history of PEQs traced along the phylogenetic tree of fossil and extant haplorhine primates; ancestral states reconstructed using maximum likelihood estimations. Both maximum likelihood estimates (numbers ahead of the slashes) and Bayesian inferences (numbers after the slashes) of the states of the most recent ancestors of the Haplorhini, anthropoids, platyrrhines, and catarrhines and the Hominini tribe are shown (summarized from fig. S6).

Acuity of visual and olfactory systems and relationship with PEQs

Chilecebus has small orbits (average diameter, 9.14 mm) compared to other primates of its body size, suggesting that it almost certainly was diurnal (*11*). With an estimated body mass of 583 g (*12*), the orbital diameter of *Chilecebus* falls well below that expected for nocturnal primates of similar size (Fig. 4A). The estimated optic foramen area of *Chilecebus* is 1.57 mm^2. Relative to estimated body mass, it is much smaller than in all other anthropoids (Fig. 4A), including the stem anthropoid *Parapithecus*.

The optic foramen index (OFI), the orbital area divided by the optic foramen area, is a measure of retinal summation (*21*, *22*), a reflection of the number of photoreceptor cells in the retina that connect with a single ganglion via vertical pathways (*23*); high summation increases light sensitivity (advantageous for nocturnal taxa) while diminishing acuity. Nocturnal haplorhines (*Aotus* and *Tarsius*) have enormous orbits and low OFIs compared to diurnal haplorhines (1.04 to 1.19 for nocturnal haplorhines versus 1.21 to 4.66 for diurnal haplorhines). The OFI of *Chilecebus* (2.40) is more than twice that of nocturnal haplorhines, falling well within the range exhibited by diurnal anthropoids (Fig. 4B). The high OFI of *Chilecebus* implies a much lower degree of retinal summation than in nocturnal haplorhines, and thus diurnal habits.

Mammals with relatively large eyes tend to be more visually acute than smaller-eyed forms (*21*, *22*). Similarly, large optic foramina correlate with greater acuity in primates (*21*, *22*). The relatively small orbits and optic foramina of the stem anthropoid, *Parapithecus*, and the stem platyrrhine, *Chilecebus*, suggest that early anthropoids were less visually acute than their living relatives (Fig. 4A). These data thus suggest that enhanced visual acuity was attained in crown platyrrhines and crown catarrhines independently, an inference that can be illuminated further by similar analyses of stem catarrhines.

The relative sizes of the optic foramen and orbit are positively and linearly correlated with PEQs in haplorhines (Supplementary Materials). The optic foramina and orbits of an outlier, *H. sapiens*, are of moderate size given its body mass, but its PEQ is vastly higher than in all other haplorhines. *Chilecebus* and *Parapithecus* have relatively small optic foramina and orbits, coupled with low PEQs, but they

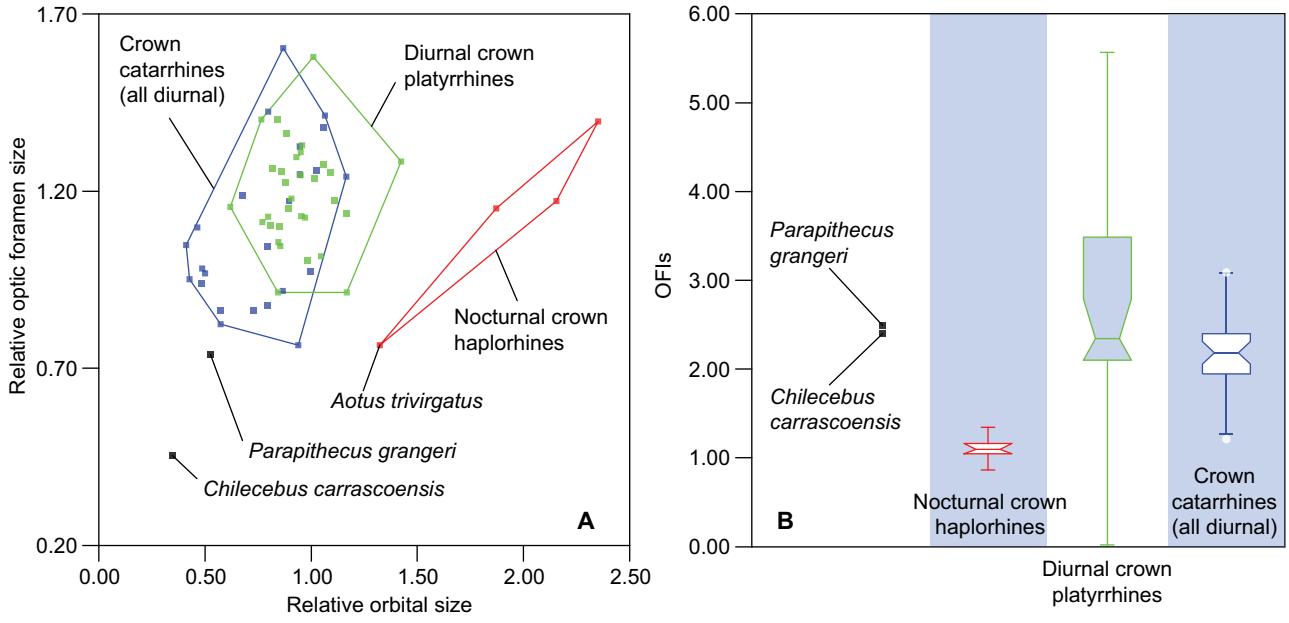

Fig. 4. Relative orbital and optic foramen sizes of fossil and extant haplorhines. (**A**) and notched box-whisker plot of the OFIs (**B**) of fossil and extant haplorhine primates. The relative orbital and optic foramen sizes were calculated by dividing the observed values by the expected values calculated from the PGLS regression for ln(orbital area) against ln(body mass) and ln(optic foramen area) against ln(body mass). OFIs were calculated by dividing orbital area by optic foramen area. Whiskers show the lowest datum within 1.5 IQR of the lower quartile and the highest datum within 1.5 IQR of the upper quartile. Outliers are shown as dots.

fall within general haplorhine trends. OFIs and PEQs show no clear correlation (Supplementary Materials).

The olfactory bulb, which develops as a small outpocketing of the telencephalon, relays olfactory information captured by the primary olfactory neurons (odor receptors) within the olfactory mucosa—specialized nasal epithelium lining the nasal cavity—to the central nervous system. The stem anthropoid *Parapithecus* and the basal catarrhine *Aegyptopithecus* both have large olfactory bulbs relative to body mass, larger than in extant tarsiers and crown platyrrhines but within the 1.5 interquartile range (IQR) of the upper quartile exhibited by extant catarrhines (fig. S7). In contrast, *Chilecebus* has an unusually small olfactory bulb, estimated as 11.1 mm^3. Relative to body mass, the olfactory bulb of *Chilecebus* is far smaller than average for extant haplorhines (fig. S7).

Transformation history of brain surface features

We examined 16 surface features of the brain seen in basal anthropoids, mapping them onto the phylogenetic tree based on phenomic features (fig. S1). Results yielded six characters supportive of platyrrhine monophyly and two characters diagnostic of catarrhines (Fig. 5). Parsimony dictates that 12 of the 16 characters arose convergently in platyrrhines and catarrhines (Fig. 5, characters 1, 2, 5, 6, 7, 8, 9, 10, 11, 14, 15, and 16). Notably, five sulci are secondarily lost in callitrichines (Fig. 5, characters 7, 9, 11, 14, and 15), consistent with their generally smooth brains relative to other anthropoids.

DISCUSSION

As one of the best-known outgroup taxa to crown platyrrhines for craniodental morphology, *Chilecebus* affords an unprecedented opportunity for reconstructing ancestral brain conditions for the extant clade and for understanding the early evolutionary transformations of the anthropoid brain more broadly. Combining data from *Chilecebus*, stem anthropoids, basal catarrhines, and platyrrhines as calibration points permits the assessment of various hypothesized evolutionary patterns of cerebral evolution in anthropoids.

The sensory system and brain are tightly coupled evolutionarily (*24*). Development of a specialized visual system and an enlarged brain are hallmarks of primate evolution (*24*). Encephalization in primates is correlated with the total amount of visual information received (*25*). Here, we use the relative size of the orbit and optic foramen as proxies for total visual input to the brain (*25*). PGLS correlations between relative optic foramen size and PEQs, and between relative orbital size and PEQs (Supplementary Materials), indicate that both features are indeed positively correlated with encephalization in anthropoids.

The size of the visual and olfactory centers of the brain is negatively correlated in extant primates, reflecting an ostensible evolutionary "trade-off" between these two regions (*24*). It is curious, therefore, that the reduced olfactory bulb in *Chilecebus* is not matched by an enhanced visual system, as reflected by orbit and optic foramen size. The olfactory bulb, orbit, and optic foramen of *Chilecebus* are all smaller (scaled to body size) than the modern anthropoid average. The lack of a statistically significant PGLS relationship between relative olfactory bulb and optic foramen size, or between relative olfactory bulb and orbital size, thus indicates that the visual and olfactory systems are less tightly coupled evolutionarily in primates than is widely assumed (*24*), with changes occurring essentially independently of each other. In addition, PGLS analysis fails to show a significant correlation between relative olfactory bulb size and PEQs in anthropoids. Even if a trend toward reduction of the olfactory system in primates exists, it is unrelated to changes in visual acuity or the degree of encephalization.

Encephalization increases in mammals have been ascribed to two potential causes. One view holds that (apart from the olfactory bulb)

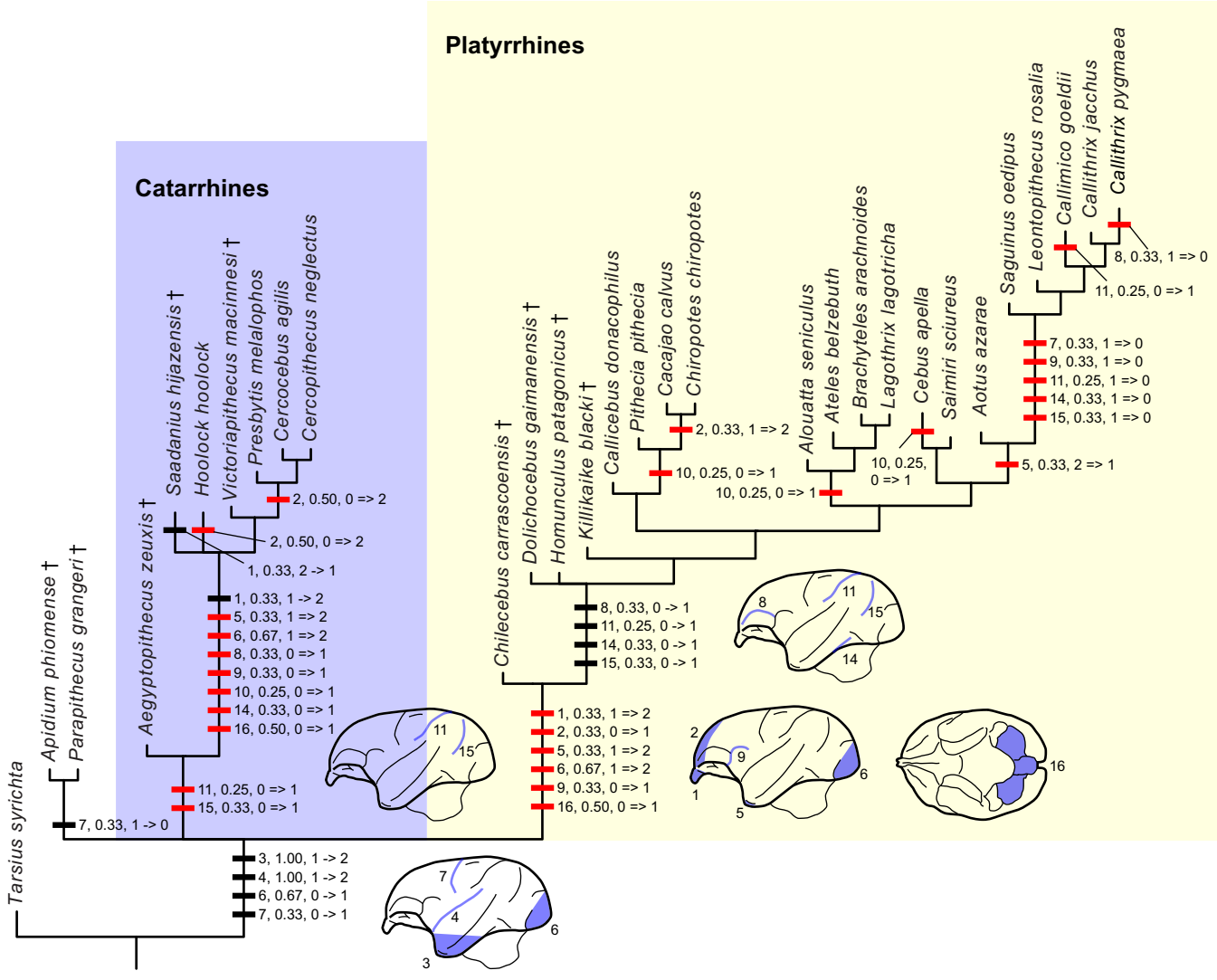

Fig. 5. Brain surface characters in tarsier and anthropoids mapped onto phylogeny emphasizing platyrrhine relationships. Apomorphic characters are mapped on the phylogenetic tree inferred from Bayesian tip dating based on the total evidence analyses of phenomic and molecular data (fig. S1). Parsimony is used for mapping the characters. Fossil taxa are indicated by † (dagger symbol). Taxa lacking preserved brain surface features are omitted. Thick horizontal bars represent a brain surface character, followed by the character's number (see below), its consistency index, and the state change. Red bars indicate unambiguously optimized. Character codes: (1), relative size of the olfactory bulb: 0, very large; 1, large; and 2, small; (2), overlap of the olfactory bulb by the frontal lobe: 0, less than half; 1, half; and 2, full; (3), expansion of the temporal lobe: 0, absent; 1, present and temporal lobe projects slightly downward; and 2, present and temporal lobe projects downward substantially; (4), Sylvian sulcus: 0, absent; 1, shallow and short; and 2, deep and long; (5), exposure of the piriform lobe in lateral view: 0, very large; 1, small; and 2, absent or very small; (6), degree to which occipital pole overlaps cerebellum: 0, none; 1, partial; and 2, fully; (7), central sulcus: 0, absent and 1, present; (8), sulcus rectus: 0, absent and 1, present; (9), arcuate sulcus: 0, absent and 1, present; (10), superior precentral sulcus: 0, absent and 1, present; (11), intraparietal sulcus: 0, absent and 1, present; (12), caudal part of the sulcus rectus approaches the intraparietal sulcus: 0, yes and 1, no; (13), superior temporal sulcus: 0, absent and 1, present; (14), inferior temporal sulcus: 0, absent and 1, present; (15), lunate sulcus: 0, absent and 1, present; (16), size of cerebellar vermis relative to cerebellar hemisphere: 0, large and 1, small.

the size of brain subdivisions, from the medulla to the forebrain, is highly but nonlinearly correlated with total brain mass (*26*). Corollaries of this view are that most major brain subdivisions covary in size and that taxonomic factors and body mass are of little consequence to encephalization. Furthermore, this view suggests that brain ontogeny is conservative across most mammal groups, potentially constraining the scaling of its components during growth. The opposing view contends that anatomical and functional components of the brain are only loosely constrained developmentally and have evolved mosaically (*24*, *27*). Perhaps the most compelling evidence favoring this view of primate brain evolution is the pronounced enlargement of the neocortex independently of other parts of the brain; accounting for scaling relationships with other brain structures, the neocortex is roughly five times more voluminous in primates than in insectivores (*24*).

Another observation favoring a highly plastic model of brain evolution concerns the scaling patterns of major subdivisions. Comparisons of the endocasts of *Chilecebus*, *Parapithecus*, *Aegyptopithecus*, *Dolichocebus*, and extant anthropoids indicate that various regions of the brain independently expanded within various clades over the

group's history. In contrast to expectations of the correlated size view, the major brain subdivisions of these early anthropoids exhibit no consistent scaling pattern relative to the overall brain size and thus appear to have transformed independently and in a mosaic fashion.

Proponents of the mosaic scenario suggest that areas of the primate brain modified late in ontogeny correspond to historically recent evolutionary shifts, while the more stable "core" areas established at early developmental stages reflect phylogenetically ancient stages of brain evolution (*28*). Extrapolating from cortical maps of extant anthropoids, the cortical regions of *Chilecebus* were likely well delimited (including primary and secondary visual areas, middle temporal area, and inferior temporal area), judging from its moderately expanded occipital and temporal lobes. These areas were likely already as advanced in *Chilecebus* as they are in contemporary anthropoids. The little expanded saddle-shaped parietal lobe of *Chilecebus*, on the other hand, argues that some areas forming during late developmental stages in extant anthropoids (e.g., the dorsomedial and third and fourth visual areas in the parietal lobe) may have been small or absent in stem platyrrhines.

Many gross anatomical features of anthropoid brains, including sulcal patterns and cortical expansion, appear to have originated in platyrrhines and catarrhines independently (*29*), a view generally consistent with the findings presented here. Others, including expansion of the frontal and occipital lobes and abundant sulci, originated convergently across different anthropoid subclades. The few brain features identified here (via phylogenetic optimization) as having been present in the last common ancestor of crown anthropoids include downward expansion of the temporal lobe, a central sulcus, and a deep Sylvian sulcus.

Although primates are widely assumed to have undergone an evolutionary trend of generally increasing brain size, recent work suggests that the pattern of encephalization is actually far more complex, involving brain size increases as well as decreases within all major primate clades (*27*). As shown above, anthropoid encephalization, as reflected in PEQ changes, has increased and decreased multiple times independently. Secondary decreases in relative brain size also are associated with simplification of sulcal patterns, at least in the case of callitrichines.

Here, we have shown that, except for in hominins, PEQs differ little across crown anthropoid lineages, whereas stem anthropoids, stem platyrrhines, and stem catarrhines all have lower PEQs. Brain size increase in hominins, however, was extraordinary and rapid. Within less than 7 Ma, PEQs of the lineage including humans and their nearest fossil allies had nearly tripled (from 4.63 to 13.64), while changes in the PEQs of their extant sister taxon, chimpanzees, were far more subdued. Profound encephalization in the human lineage has molecular correlates: Genes of the nervous system exhibit a more dynamic pattern of molecular evolutionary change in humans than in chimpanzees and other primates (*30*–*32*). Collectively, these observations imply that evolutionary change of the nervous system is driven by fundamentally different pressures in the human lineage than in other anthropoids.

MATERIALS AND METHODS

High-resolution CT scanning was performed at the Center for Quantitative Imaging at Pennsylvania State University using the X-TEK x-ray system. *Chilecebus* was scanned in the coronal plane. The dataset consisted of a 16-bit grayscale volume of 1024 × 1024 × 1148 voxels. Voxel dimensions were 0.04 × 0.04 × 0.04641 mm. Segmentation and 3D reconstruction processes followed procedures described elsewhere (*33*). VGStudio Max 2.2 was used for 3D visualization.

We used both Bayesian tip dating and parsimony-based criterion to infer the phylogeny. The PEQ, developed for this study, is the ratio between the actual (E_a) and expected (E_e) brain size for a species of a given body mass from allometric brain-body mass scaling from PGLS regression of data from living anthropoids (Fig. 3). PEQ = E_a/E_e, where $E_e = 0.42(\text{body mass})^{0.50}$.

Relative orbit, optic foramen, and olfactory bulb size were defined as the quotients of the observed values and the expected values derived from PGLS fittings for the allometric relationships of orbit area against body mass, optic foramen area against body mass, and olfactory bulb weight against body mass. We optimized brain surface characters onto the Bayesian tip dating tree under a parsimony ACCTRAN framework using PAUP* (*34*) to determine transformation sequences.

SUPPLEMENTARY MATERIALS

Supplementary material for this article is available at http://advances.sciencemag.org/cgi/content/full/5/8/eaav7913/DC1

Phylogenetic analysis based on phenetic and molecular characters
Composite phylogenetic tree and estimated divergence times
Virtual endocranial cast of *C. carrascoensis*
Measurements of the virtual endocranial cast of *C. carrascoensis*
Comparison of lateral profiles of endocranial casts
Allometric relationship between brain and body mass
Tracing PEQs along the composite phylogenetic tree
Estimating acuity of the visual sensory system
Estimating acuity of the olfactory sensory system
Fig. S1. Tree topology and divergence times of anthropoids inferred from Bayesian tip dating.
Fig. S2. Strict consensus of six most parsimonious phylogenetic trees.
Fig. S3. Majority consensus of six most parsimonious phylogenetic trees.
Fig. S4. Virtual endocranial cast of *C. carrascoensis* based on high-resolution x-ray CT scanning images.
Fig. S5. Comparison of the lateral profile of the endocranial cast of *C. carrascoensis* with other anthropoids.
Fig. S6. Tracing PEQs along the composite phylogenetic tree of fossil and extant haplorhine primates (data file S4).
Fig. S7. Notched box-whisker plot of the relative olfactory bulb size of fossil and extant haplorhine primates.
Table S1. Measurements of the virtual endocranial cast of *C. carrascoensis* [mm, mm^2 (areas), or mm^3 (volumes)].
Data file S1. Data matrix used for phylogenetic analysis (in NEXUS format).
Data file S2. MrBayes commands used for Bayesian tip dating analysis.
Data file S3. Fossil age, estimated divergence times, and branch length of selected fossil anthropoids.
Data file S4. The composite phylogenetic tree with estimated divergence times in NEXUS format.
Data file S5. Body mass and brain weight of extant and fossil haplorhine primates.
Data file S6. Regressions for ln(brain mass) and ln(body mass) in anthropoids, catarrhines, and platyrrhines.
Data file S7. PEQ, body mass, optic foramen area, orbital area, OFI, relative optic foramen size, and relative orbital size of extant and fossil haplorhine primates.
Data file S8. Regressions used for estimating acuity of the visual sensory system and the olfactory sensory system.
Data file S9. Body mass, brain mass, PEQ, olfactory bulb mass, and relative olfactory bulb size of extant and fossil haplorhine primates.
References (*35*–*84*)

REFERENCES AND NOTES

1. L. Radinsky, The fossil evidence of anthropoid brain evolution. *Am. J. Phys. Anthropol.* **41**, 15–27 (1974).
2. T. B. Rowe, T. E. Macrini, Z.-X. Luo, Fossil evidence on origin of the mammalian brain. *Science* **332**, 955–957 (2011).
3. L. E. Powell, K. Isler, R. A. Barton, Re-evaluating the link between brain size and behavioural ecology in primates. *Proc. R. Soc. Lond. B Biol. Sci.* **284**, 20171765 (2017).

4. A. R. DeCasien, S. A. Williams, J. P. Higham, Primate brain size is predicted by diet but not sociality. *Nat. Ecol. Evol.* **1**, 0112 (2017).
5. S. L. Gilbert, W. B. Dobyns, B. T. Lahn, Genetic links between brain development and brain evolution. *Nat. Rev. Genet.* **6**, 581–590 (2005).
6. C. Ponting, A. P. Jackson, Evolution of primary microcephaly genes and the enlargement of primate brains. *Curr. Opin. Genet. Dev.* **15**, 241–248 (2005).
7. R. Bauchot, H. Stephan, Encéphales et moulages endocraniens de quelques insectivores et primates actuels. *Colloq. Inter. Cent. Nat. Rech. Sci.* **163**, 575–586 (1967).
8. M. Bond, M. F. Tejedor, K. E. Campbell Jr., L. Chornogubsky, N. Novo, F. Goin, Eocene primates of South America and the African origins of New World monkeys. *Nature* **520**, 538–541 (2015).
9. E. B. Ottoni, P. Izar, Capuchin monkey tool use: Overview and implications. *Evol. Anthropol.* **17**, 171–178 (2008).
10. P. Hershkovitz, *Living New World Monkeys (Platyrrhini): With an Introduction to Primates* (University of Chicago Press, 1977).
11. J. J. Flynn, A. R. Wyss, R. Charrier, C. C. Swisher, An early Miocene anthropoid skull from the Chilean Andes. *Nature* **373**, 603–607 (1995).
12. K. E. Sears, J. A. Finarelli, J. J. Flynn, A. R. Wyss, Estimating body mass in New World "monkeys" (Platyrrhini, Primates), with a consideration of the Miocene platyrrhine, *Chilecebus carrascoensis*. *Am. Mus. Novit.* **3617**, 1–29 (2008).
13. G. C. Conroy, Evolutionary significance of cerebral venous patterns in paleoprimatology. *Z. Morphol. Anthropol.* **71**, 125–134 (1980).
14. R. F. Kay, J. G. Fleagle, T. R. T. Mitchell, M. Colbert, T. Bown, D. W. Powers, The anatomy of *Dolichocebus gaimanensis*, a stem platyrrhine monkey from Argentina. *J. Hum. Evol.* **54**, 323–382 (2008).
15. X. Ni, D. L. Gebo, M. Dagosto, J. Meng, P. Tafforeau, J. J. Flynn, K. C. Beard, The oldest known primate skeleton and early haplorhine evolution. *Nature* **498**, 60–64 (2013).
16. E. C. Bush, E. L. Simons, J. M. Allman, High-resolution computed tomography study of the cranium of a fossil anthropoid primate, *Parapithecus grangeri*: New insights into the evolutionary history of primate sensory systems. *Anat. Rec.* **281A**, 1083–1087 (2004).
17. E. L. Simons, E. R. Seiffert, T. M. Ryan, Y. Attia, A remarkable female cranium of the early Oligocene anthropoid *Aegyptopithecus zeuxis* (Catarrhini, Propliopithecidae). *Proc. Natl. Acad. Sci. U.S.A.* **104**, 8731–8736 (2007).
18. E. L. Simons, New endocasts of *Aegyptopithecus*: Oldest well-preserved record of the brain in anthropoidea. *Am. J. Sci.* **293-A**, 383–390 (1993).
19. H. J. Jerison, Brain, body and encephalization in early Primates. *J. Hum. Evol.* **8**, 615–635 (1979).
20. E. Paradis, *Analysis of Phylogenetics and Evolution with R* (Springer, ed. 2, 2012).
21. R. F. Kay, E. C. Kirk, Osteological evidence for the evolution of activity pattern and visual acuity in primates. *Am. J. Phys. Anthropol.* **113**, 235–262 (2000).
22. E. C. Kirk, R. F. Kay, in *Anthropoid Origins: New Visions*, C. F. Ross, R. F. Kay, Eds. (Kluwer Academic/Plenum Publishers, 2004), pp. 539–602.
23. G. L. Walls, *The Vertebrate Eye and Its Adaptive Radiation* (Bulletin 19, The Cranbrook Institute of Science, 1942).
24. R. A. Barton, Primate brain evolution: Integrating comparative, neurophysiological, and ethological data. *Evol. Anthropol.* **15**, 224–236 (2006).
25. E. C. Kirk, Visual influences on primate encephalization. *J. Hum. Evol.* **51**, 76–90 (2006).
26. K. E. Yopak, T. J. Lisney, R. B. Darlington, S. P. Collin, J. C. Montgomery, B. L. Finlay, A conserved pattern of brain scaling from sharks to primates. *Proc. Natl. Acad. Sci. U.S.A.* **107**, 12946–12951 (2010).
27. J. B. Smaers, C. Soligo, Brain reorganization, not relative brain size, primarily characterizes anthropoid brain evolution. *Proc. R. Soc. Lond. B Biol. Sci.* **280**, 20130269 (2013).
28. M. G. P. Rosa, R. Tweedale, Brain maps, great and small: Lessons from comparative studies of primate visual cortical organization. *Philos. Trans. R. Soc. Lond. B Biol. Sci.* **360**, 665–691 (2005).
29. D. Falk, in *Evolutionary Biology of the New World Monkeys and Continental Drift*, R. L. Ciochon, A. B. Chiarelli, Eds. (Plenum Press, 1981), pp. 275–292.
30. S. Dorus, E. J. Vallender, P. D. Evans, J. R. Anderson, S. L. Gilbert, M. Mahowald, G. J. Wyckoff, C. M. Malcom, B. T. Lahn, Accelerated evolution of nervous system genes in the origin of *Homo sapiens*. *Cell* **119**, 1027–1040 (2004).
31. C. Tyler-Smith, Y. Xue, Sibling rivalry among paralogs promotes evolution of the human brain. *Cell* **149**, 737–739 (2012).
32. Y. E. Zhang, P. Landback, M. Vibranovski, M. Long, New genes expressed in human brains: Implications for annotating evolving genomes. *Bioessays* **34**, 982–991 (2012).
33. X. Ni, J. J. Flynn, A. R. Wyss, Imaging the inner ear in fossil mammals: High-resolution CT scanning and 3-D virtual reconstructions. *Palaeontol. Electronica* **15**, 18A (2012).
34. D. L. Swofford, *PAUP*. Phylogenetic Analysis Using Parsimony (*and Other Methods)* (Sinauer Associates, 2002).
35. M. S. Springer, R. W. Meredith, J. Gatesy, C. A. Emerling, J. Park, D. L. Rabosky, T. Stadler, C. Steiner, O. A. Ryder, J. E. Janečka, C. A. Fisher, W. J. Murphy, Macroevolutionary dynamics and historical biogeography of primate diversification inferred from a species supermatrix. *PLOS ONE* **7**, e49521 (2012).
36. W. P. Maddison, D. R. Maddison, *Mesquite: A Modular System for Evolutionary Analysis. Version 3.51* (2018).
37. F. Ronquist, M. Teslenko, P. van der Mark, D. L. Ayres, A. Darling, S. Höhna, B. Larget, L. Liu, M. A. Suchard, J. P. Huelsenbeck, MrBayes 3.2: Efficient Bayesian phylogenetic inference and model choice across a large model space. *Syst. Biol.* **61**, 539–542 (2012).
38. P. O. Lewis, A likelihood approach to estimating phylogeny from discrete morphological character data. *Syst. Biol.* **50**, 913–925 (2001).
39. Z. Yang, Maximum likelihood phylogenetic estimation from DNA sequences with variable rates over sites: Approximate methods. *J. Mol. Evol.* **39**, 306–314 (1994).
40. C. Zhang, F. Ronquist, S. Klopfstein, T. Stadler, T. A. Heath, Total-evidence dating under the fossilized birth–death process. *Syst. Biol.* **65**, 228–249 (2015).
41. F. Ronquist, S. Klopfstein, L. Vilhelmsen, S. Schulmeister, D. L. Murray, A. P. Rasnitsyn, A total-evidence approach to dating with fossils, applied to the early radiation of the hymenoptera. *Syst. Biol.* **61**, 973–999 (2012).
42. E. R. Seiffert, E. L. Simons, J. G. Fleagle, M. Godinot, in *Cenozoic Mammals of Africa*, L. Werdelin, W. J. Sanders, Eds. (University of California Press, 2010), pp. 369–391.
43. M. A. O'Leary, J. I. Bloch, J. J. Flynn, T. J. Gaudin, A. Giallombardo, N. P. Giannini, S. L. Goldberg, B. P. Kraatz, Z.-X. Luo, J. Meng, X. Ni, M. J. Novacek, F. A. Perini, Z. S. Randall, G. W. Rougier, E. J. Sargis, M. T. Silcox, N. B. Simmons, M. Spaulding, P. M. Velazco, M. Weksler, J. R. Wible, A. L. Cirranello, The placental mammal ancestor and the Post–K-Pg radiation of placentals. *Science* **339**, 662–667 (2013).
44. T. Lepage, D. Bryant, H. Philippe, N. Lartillot, A general comparison of relaxed molecular clock models. *Mol. Biol. Evol.* **24**, 2669–2680 (2007).
45. C. Lakner, P. van der Mark, J. P. Huelsenbeck, B. Larget, F. Ronquist, Efficiency of Markov chain Monte Carlo tree proposals in Bayesian phylogenetics. *Syst. Biol.* **57**, 86–103 (2008).
46. A. Rambaut, A. J. Drummond, D. Xie, G. Baele, M. A. Suchard, Posterior summarization in bayesian phylogenetics using Tracer 1.7. *Syst. Biol.* **67**, 901–904 (2018).
47. P. A. Goloboff, J. S. Farris, K. C. Nixon, TNT, a free program for phylogenetic analysis. *Cladistics* **24**, 774–786 (2008).
48. K. Bremer, Branch support and tree stability. *Cladistics* **10**, 295–304 (1994).
49. P. A. Goloboff, J. S. Farris, Methods for quick consensus estimation. *Cladistics* **17**, S26–S34 (2001).
50. R. F. Kay, Biogeography in deep time—What do phylogenetics, geology, and paleoclimate tell us about early platyrrhine evolution? *Mol. Phylogenet. Evol.* **82**, 358–374 (2015).
51. D. S. Strait, F. E. Grine, J. G. Fleagle, Analyzing hominid phylogeny, in *Handbook of Paleoanthropology*, W. Henke, I. Tattersall, Eds. (Springer, 2007), pp. 1781–1806.
52. E. Delson, P. Andrews, in *Encyclopedia of Human Evolution and Prehistory*, E. Delson, I. Tattersall, J. A. Van Couvering, A. S. Brooks, Eds. (Garland Publishing Inc., 2000), pp. 221–222.
53. D. R. Begun, in *The Primate Fossil Record*, W. C. Hartwig, Ed. (Cambridge Univ. Press, 2002), pp. 339–368.
54. D. R. Begun, Fossil record of Miocene hominoids, in *Handbook of Paleoanthropology*, W. Henke, I. Tattersall, Eds. (Springer, 2007), pp. 921–977.
55. B. R. Benefit, M. L. McCrossin, Earliest known Old World monkey skull. *Nature* **388**, 368–371 (1997).
56. E. Delson, C. J. Terranova, W. L. Jungers, E. J. Sargis, N. G. Jablonski, P. C. Dechow, Body mass in Cercopithecidae (Primates, Mammalia): Estimation and scaling in extinct and extant taxa. *Anthropol. Pap. Am. Mus.Nat. Hist.* **83**, 1–159 (2000).
57. S. Elton, L. C. Bishop, B. Wood, Comparative context of Plio-Pleistocene hominin brain evolution. *J. Hum. Evol.* **41**, 1–27 (2001).
58. D. Falk, Evolution of the primate brain, in *Handbook of Paleoanthropology*, W. Henke, I. Tattersall, Eds. (Springer, 2007), pp. 1133–1162.
59. T. Harrison, in *The Primate Fossil Record*, W. C. Hartwig, Ed. (Cambridge Univ. Press, 2002), pp. 311–338.
60. K. Harvati, S. Frost, Dental eruption sequences in fossil colobines and the evolution of primate life histories. *Int. J. Primatol.* **28**, 705–728 (2007).
61. D. Jablonski, Survival without recovery after mass extinctions. *Proc. Natl. Acad. Sci. U.S.A.* **99**, 8139–8144 (2002).
62. R. F. Kay, J. M. G. Perry, M. Malinzak, K. L. Allen, E. C. Kirk, J. M. Plavcan, J. G. Fleagle, in *Early Miocene Paleobiology in Patagonia: High-Latitude Paleocommunities of the Santa Cruz Formation*, S. F. Vizcaino, R. F. Kay, M. S. Bargo, Eds. (Cambridge Univ. Press, 2012), pp. 306–330.
63. E. R. Seiffert, Revised age estimates for the later Paleogene mammal faunas of Egypt and Oman. *Proc. Natl. Acad. Sci. U.S.A.* **103**, 5000–5005 (2006).
64. E. M. Weston, A. M. Lister, Insular dwarfism in hippos and a model for brain size reduction in *Homo floresiensis*. *Nature* **459**, 85–88 (2009).
65. T. D. White, B. Asfaw, Y. Beyene, Y. Haile-Selassie, C. O. Lovejoy, G. Suwa, G. WoldeGabriel, *Ardipithecus ramidus* and the paleobiology of early hominids. *Science* **326**, 64, 75–86 (2009).
66. D. R. Begun, L. Kordos, in *The Evolution of Thought: Evolutionary Origins of Great Ape Intelligence*, A. E. Russon, D. R. Begun, Eds. (Cambridge Univ. Press, 2004), pp. 260–279.

67. J. G. Fleagle, *Primate Adaptation and Evolution* (Academic Press, ed. 2, 1999), p. 596.
68. F. Guy, D. E. Lieberman, D. Pilbeam, M. P. de Leon, A. Likius, H. T. Mackaye, P. Vignaud, C. Zollikofer, M. Brunet, Morphological affinities of the *Sahelanthropus tchadensis* (Late Miocene hominid from Chad) cranium. *Proc. Natl. Acad. Sci. U.S.A.* **102**, 18836–18841 (2005).
69. T. Harrison, A reassessment of the phylogenetic relationships of *Oreopithecus bambolii* gervais. *J. Hum. Evol.* **15**, 541–583 (1986).
70. P. H. Harvey, R. D. Martin, T. H. Clutton-Brock, in *Primate Societies*, B. B. Smuts, D. L. Cheney, R. M. Seyfarth, R. W. Wrangham, T. T. Struhsaker, Eds. (University of Chicago Press, 1987), pp. 181–196.
71. H. Hemmer, Estimation of basic life history data of fossil hominoids, in *Handbook of Paleoanthropology* (Springer, 2007), pp. 587–619.
72. R. L. Holloway, D. C. Broadfield, M. S. Yuan, *The Human Fossil Record: Brain Endocasts* (John Wiley & Sons Inc., 2004), p. 315.
73. K. Isler, E. Christopher Kirk, J. M. A. Miller, G. A. Albrecht, B. R. Gelvin, R. D. Martin, Endocranial volumes of primate species: Scaling analyses using a comprehensive and reliable data set. *J. Hum. Evol.* **55**, 967–978 (2008).
74. R. D. Martin, in *Theropithecus. The Rise and Fall of a Primate Genus*, N. G. Jablonski, Ed. (Cambridge Univ. Press, 1993), pp. 273–298.
75. M. C. Nargolwalla, D. R. Begun, M. C. Dean, D. J. Reid, L. Kordos, Dental development and life history in *Anapithecus hernyaki*. *J. Hum. Evol.* **49**, 99–121 (2005).
76. E. L. Simons, D. T. Rasmussen, Skull of *Catopithecus browni*, an early Tertiary catarrhine. *Am. J. Phys. Anthropol.* **100**, 261–292 (1996).
77. E. L. Simons, Preliminary description of the cranium of *Proteopithecus sylviae*, an Egyptian late Eocene anthropoidean primate. *Proc. Natl. Acad. Sci. U.S.A.* **94**, 14970–14975 (1997).
78. E. L. Simons, in *Anthropoid Origins*, C. F. Ross, R. F. Kay, Eds. (Kluwer Academic/Plenum Publishers, 2004), pp. 183–204.
79. R. J. Smith, W. L. Jungers, Body mass in comparative primatology. *J. Hum. Evol.* **32**, 523–559 (1997).
80. R Core Team, *R: A language and environment for statistical computing.* (R Foundation for Statistical Computing, 2018).
81. L. J. Revell, phytools: An R package for phylogenetic comparative biology (and other things). *Methods Ecol. Evol.* **3**, 217–223 (2012).
82. H. Stephan, H. Frahm, G. Baron, New and revised data on volumes of brain structures in insectivores and primates. *Folia Primatol.* **35**, 1–29 (1981).
83. R. A. Barton, A. Purvis, P. H. Harvey, Evolutionary radiation of visual and olfactory brain systems in primates, bats and insectivores. *Philos. Trans. R. Soc. Lond. B Biol. Sci.* **348**, 381–392 (1995).
84. R. A. Barton, Olfactory evolution and behavioral ecology in primates. *Am. J. Primatol.* **68**, 545–558 (2006).

Acknowledgments: We thank T. Ryan and A. Walker of Penn State University and the PSU Center for Quantitative Imaging for CT scanning. We are grateful for the long-term support of the Museo Nacional de Historia Natural (Santiago, Chile) and the Consejo Nacional de Monumentos Naturales de Chile. **Funding:** This project has been supported by the Strategic Priority Research Program of the Chinese Academy of Sciences (CAS XDB26030300 and XDA20070203-19050100 to X.N.), the National Natural Science Foundation of China (41472025-41625005 to X.N.), the External Cooperation Program of BIC of the Chinese Academy of Sciences (132311KYSB20160008 to X.N.), the U.S. National Science Foundation (DEB-9317943, DEB-0317014, and DEB-0513476 to J.J.F.; DEB-9020213 and DEB-9318126 to A.R.W.), and a John S. Guggenheim Memorial Foundation Fellowship (to J.J.F.). **Author contributions:** X.N., J.J.F., and A.R.W. made extensive contributions. C.Z. and X.N. performed Bayesian tip dating analyses; X.N. performed the parsimony-based phylogenetic and statistical analyses. **Competing interests:** The authors declare that they have no competing interests. **Data and materials availability:** All data needed to evaluate the conclusions in the paper are present in the paper and/or the Supplementary Materials.

Submitted 22 October 2018
Accepted 15 July 2019
Published 21 August 2019
10.1126/sciadv.aav7913

Citation: X. Ni, J. J. Flynn, A. R. Wyss, C. Zhang, Cranial endocast of a stem platyrrhine primate and ancestral brain conditions in anthropoids. *Sci. Adv.* **5**, eaav7913 (2019).